Inorganic Chemistry

Article

pubs.acs.org/IC

Framework Complexes of Group 2 Metals Organized by Homochiral Rods and $\pi\cdots\pi$ Stacking Forces: A Breathing Supramolecular MOF

Daniel L. Reger,* Andrew Leitner, Perry J. Pellechia, and Mark D. Smith

Department of Chemistry and Biochemistry, University of South Carolina, Columbia, South Carolina 29208, United States

Supporting Information

ABSTRACT: The reactions of the potassium salts of the ligands (*S*)-2-(1,8-naphthalimido)propanoate (KL_{ala}), (*S*)-2-(1,8-naphthalimido)-3-hydroxypropanoate (KL_{ser}), and (*R*)-2-(1,8-naphthalimido)propanoate (KL_{ala}*), enantiopure carboxylate ligands containing a 1,8-naphthalimide $\pi\cdots\pi$ stacking supramolecular tecton, and, in the case of L_{ser}^-, an alcohol functional group with calcium or strontium nitrate under solvothermal conditions produce crystalline $[Ca(L_{ala})_2(H_2O)]\cdot(H_2O)$ (**1**); $[Ca(L_{ser})_2]\cdot(H_2O)_2$ (**2**); $[Sr(L_{ala})_2(H_2O)]\cdot(H_2O)_3$ (**3**); $[Sr(L_{ala}*)_2(H_2O)]\cdot(H_2O)_3$ (**3***); and $[Sr(L_{ser})_2(H_2O)]$ (**5**). Placing **3** under vacuum removes the interstitial waters to produce $[Sr(L_{ala})_2(H_2O)]$ (**4**) in a single-crystal to single-crystal transformation; introduction of water vapor to **4** leads to the reformation of crystalline **3**. Each of these new complexes has a solid-state structure based on homochiral rod secondary building unit (SBUs) central cores. Supramolecular $\pi\cdots\pi$ stacking interactions between 1,8-naphthalimide rings link adjacent rod SBUs into three-dimensional structures for **1**, **3**, **4**, and **5** and two-dimensional structure for **2**. Compounds **1** and **3** have open one-dimensional channels along the crystallographic *c* axis that are occupied by disordered solvent. For **3**, these channels close and open in the reversible single-crystal conversion to **4**; the $\pi\cdots\pi$ stacking interactions of the naphthalimide rings facilitate this process by rotating and slipping. Infrared spectroscopy demonstrated that the rehydration of **4** with D_2O leads to $\mathbf{3d_8}$, and the process of dehydration and rehydration of $\mathbf{3d_8}$ with H_2O leads to **3**, thus showing exchange of the coordinated water in this process. These forms of **3** and **4** were characterized by ^1H, ^2H, and ^{13}C solid-state NMR spectroscopy, and thermal and luminescence data are reported on all of the complexes.

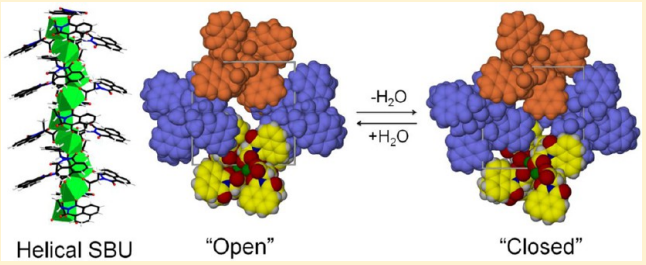

INTRODUCTION

The crystal engineering of metal−organic hybrid materials with novel extended structures remains an important goal in synthesis and crystal growth.[1] Metal−organic frameworks (MOFs) are composed of groups of metal ions, also known as secondary building units (SBUs), covalently connected in one, two, or three dimensions by organic linkers.[2] Supramolecular tectons (e.g., groups that can hydrogen bond or participate in $\pi\cdots\pi$ stacking interactions) can be built into the bridging ligands for enhanced flexibility and stability.[3] Flexible MOFs can show reversible structural changes based on external stimuli and have shown selective adsorption of substrates that can be used for sensing and separations.[4] The ability to characterize these highly flexible crystalline materials by solid-state NMR spectroscopy has been well established.[4a,5]

We have designed a series of ligands (Scheme 1) containing a carboxylate donor group and a naphthalimide $\pi\cdots\pi$ stacking supramolecular tecton. Of interest here are the ligands derived from enantiopure naturally occurring amino acids that all contain a single carboxylate group that coordinates to the metals to create the SBUs and a chiral center that imparts its chirality on the SBU, leading to solids in noncentrosymmetric space groups.[3,6,7] Using amino acid precursors provides access to additional functionality made available by the side-chain, varying in the work reported here from a methyl group in the case of L-alanine (in one case, R-alanine) to a hydroxyl group, in the case of L-serine. Most complexes of amino acid ligands involve coordination of the amine to the metal.[8] We avoid this coordination by protecting the amine with a 1,8-naphthalimide group that not only blocks it from coordination but also has a propensity to engage in strong $\pi\cdots\pi$ stacking interactions, which have a substantial impact on the three-dimensional (3D) structures.[6,9,10] The 1,8-naphthalimide group is also an excellent chromophore that has many biological imaging applications including probing, cellular imaging, and DNA-tagging for anticancer research because of the ability to form strong intermolecular complexes with nucleic acids.[11]

Scheme 1. Multifunctional Ligands

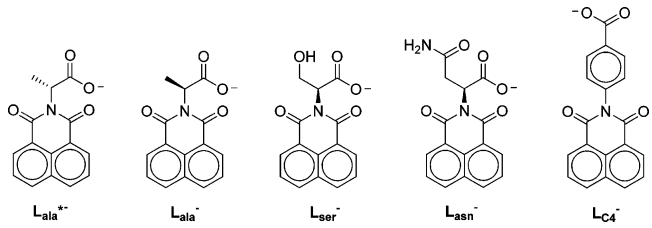

Received: July 3, 2014
Published: August 26, 2014

   dx.doi.org/10.1021/ic501581c | Inorg. Chem. 2014, 53, 9932−9945

When these ligands are combined with transition metals, the three-dimensional structures of the new complexes are generally dominated by $\pi\cdots\pi$ stacking and contain either open channels or cavities filled with disordered solvent.[6] These solids have interesting and potentially useful properties. For example, in a previous paper, we showed a densely packed compound held together by $\pi\cdots\pi$ stacking, $[Zn_2(\mathbf{L}_{C4})_4(DMSO)_2]\cdot 2(CH_2Cl_2)$, could exchange interstitial dichloromethane for water, despite the lack of pores, via a single-crystal to single-crystal transformation.[9a] In a separate paper, we showed enantioselective binding of racemic ethyl lactate to the copper paddlewheel SBU in the compound $[Cu_4(\mathbf{L}_{asn})_8(pyridine)(MeOH)]$, also via a single-crystal to single-crystal transformation.[6c] When $\mathbf{L}_{ala}^-$ and $\mathbf{L}_{ser}^-$ are combined with group 1 metals, the structures are dominated by the consistent formation of helical rod SBUs that are in all cases homochiral.[7] These MOFs have been shown to be thermally stable, as they retain single-crystallinity even after being heated to 200 °C in air. In addition, the compounds $Na(\mathbf{L}_{ala})(H_2O)$ and $K(\mathbf{L}_{ala})(H_2O)$ show interesting flexibility; bridging water molecules of the rod-shaped SBU can be reversibly removed, despite coordination to two metals, in single-crystal to single-crystal transformations. The combination of the homochiral rod-shaped SBUs and naphthalimide groups opened up the possibilities for unique electronic properties, which we demonstrated with modest solid-state luminescence and second-order harmonic generation.

There has been limited research on the synthesis of MOFs from s-block metals with little previous ability to predict and control the coordination geometry, let alone control the formation of the SBU in MOF-type structures.[12] Given our success with group 1 complexes of $\mathbf{L}_{ala}^-$ and $\mathbf{L}_{ser}^-$ (Scheme 1), where we showed the consistent formation of rare examples of homochiral rod SBUs,[2] we decided to investigate the dicationic metals in group 2. We report here the syntheses of complexes of calcium and strontium with these same two enantiopure ligands, and, in one case, with the enantiomeric ligand $\mathbf{L}_{ala}{}^{*-}$. As observed in the group 1 complexes, the structures of these compounds are dominated by homochiral rod SBUs. In contrast to the group 1 chemistry where both 3D and two-dimensional (2D) MOF structures formed, with these group 2 metals only one-dimensional (1D) structures form, but the $\pi\cdots\pi$ stacking interactions lead to supramolecular MOFs (SMOFs) in which the remaining dimensions are organized by noncovalent forces. In one case, the strontium polyhedra adopt a rare face sharing configuration that composes the rod-shaped SBU.[13] Another of the compounds undergoes a dynamic single-crystal to single-crystal transformation; a breathing SMOF in which the 1D channels can be open or closed. The nature of this breathing was investigated by single-crystal X-ray crystallography and by infrared (IR) and solid-state ^1H, ^{13}C, and ^2H NMR spectroscopy. In addition, we report the thermal and luminescent properties of these complexes.

EXPERIMENTAL SECTION

General Considerations. All reactants were used as purchased from Aldrich and Strem. The syntheses of the ligand precursors $H\mathbf{L}_{ala}$ and $H\mathbf{L}_{ser}$ have been reported elsewhere.[7] $H\mathbf{L}_{ala}{}^*$ is synthesized the same as $H\mathbf{L}_{ala}$ but starts with D-alanine instead of the naturally occurring L-alanine to produce the protonated ligand with the opposite handed chirality. Elemental analyses were performed by Robertson Microlit Laboratories (Ledgewood, NJ). ^1H, ^{13}C, and ^2H solid-state NMR spectra were recorded on a Bruker Advance III-HD 500 MHz spectrometer. Infrared spectra were recorded on a Thermo Nicolet Avatar 360 FT-IR spectrophotometer. Crystals were collected and transferred to a drybox, ground into a Nujol mull, and placed between NaCl plates. Thermalgravimetric analyses were performed using a thermal analysis (TA) SDT Q600 simultaneous DTA/TGA system. The samples were heated in dry air to 800 °C with a heating rate of 10 °C/min. For compound **1**, the experiment was terminated after the decomposition temperature was recorded because the compound frothed when heated to decomposition. The fluorescence measurements were done on a PerkinElmer Lambda 35 UV−vis spectrometer.

$[Ca(\mathbf{L}_{ala})_2(H_2O)]\cdot(H_2O)$ (1). $H\mathbf{L}_{ala}$ (2.0 g, 7.4 mmol) was added to a solution of potassium hydroxide (0.42 g, 7.4 mmol) in water (25 mL) and stirred for 1 h until the solution was homogeneous. The solvent was evaporated, and the remaining solid was dried in vacuo to produce the potassium salt of the ligand ($K\mathbf{L}_{ala}$) as a light brown powder (1.96 g). A 9 mL thick walled glass tube with a Teflon screw top was charged with a sample of this solid (0.055 g), calcium nitrate tetrahydrate (0.017 g, 0.075 mmol), and 1 mL of a 1:1 water/isopropanol solution, and the mixture was heated at 120 °C. Over the course of heating for 3 days, yellow crystals grew on the walls of the tube above the solvent line. After no starting material remained at the bottom of the tube, the heat was removed, and the system was allowed to slowly cool at a rate of about 1 °C/min. Small yellow crystals were collected from the walls of the tube and washed with diethyl ether to provide 0.031 g of single crystals. Anal. calcd (found) for $C_{30}H_{24}CaN_2O_{10}$: C 58.98 (58.92); H 3.79 (4.02); N 4.58 (4.34).

$[Ca(\mathbf{L}_{ser})_2]\cdot(H_2O)_2$ (2). This complex was prepared as for **1** using $K\mathbf{L}_{ser}$ (0.050 g), calcium nitrate tetrahydrate (0.010 g, 0.061 mmol) and 1 mL of a 1:1 water/isopropanol solution to produce colorless crystals that were washed with methanol to provide 0.026 g of single crystals. Crystals were dried to constant weight before elemental analysis. Anal. calcd (found) for $C_{30}H_{24}CaN_2O_{12}$: C 55.90 (56.29); H 3.75 (4.05); N 4.34 (4.83).

$[Sr(\mathbf{L}_{ala})_2(H_2O)]\cdot(H_2O)_3$ (3). A 9 mL thick walled glass tube with a Teflon screw top was charged with $K\mathbf{L}_{ala}$ (0.050 g), anhydrous strontium nitrate (0.015 g, 0.070 mmol), and 1 mL of a 4:1 water/methanol solution and heated at 120 °C. Yellow crystals grew overnight on the walls of the tube above the solvent line. Small yellow crystals were collected and washed with methanol to provide 0.028 g of single crystals. Anal. calcd (found) for $C_{30}H_{28}N_2O_{12}Sr$: C 51.72 (52.09); H 4.06 (3.84); N 4.02 (3.89).

$[Sr(\mathbf{L}_{ala}{}^*)_2(H_2O)]\cdot(H_2O)_3$ (3*). This compound was prepared by the same procedure as for **3** but started with $K\mathbf{L}_{ala}{}^*$.

$[Sr(\mathbf{L}_{ser})_2(H_2O)]$ (5). This compound was prepared by the same procedure as for **2**, but used $Sr(NO_3)_2$ (0.032 g), $K\mathbf{L}_{ser}$ (0.115 g), and 1 mL of a 1:9 water isopropanol solution to produce large colorless needles. Colorless crystals were collected from the walls of the tube and washed with methanol to provide 0.060 g of single crystals. Crystals were dried to constant weight before elemental analysis. Anal. calcd (found) for $C_{30}H_{22}N_2O_{11}Sr$: C 53.42 (53.45); H 3.02 (3.29); N 4.16 (4.16).

Single-Crystal to Single-Crystal Experiments—Synthesis of $[Sr(\mathbf{L}_{ala})_2(H_2O)]$ (4). Compound **3** undergoes a reversible single-crystal to single-crystal transformation when placed under vacuum to form $[Sr(\mathbf{L}_{ala})_2(H_2O)]$ (**4**). Single crystals of compound **3** were collected from the walls of the solvothermal tubes and washed with methanol. After checking the unit cell with single crystal X-ray diffraction to verify crystallinity, we held the crystals under vacuum for 1 h, and single crystal X-ray diffraction showed that compound **4** had formed, although the crystallinity was degraded. Anal. calcd (found) for $C_{30}H_{22}N_2O_9Sr$: C 56.11 (56.50); H 3.45 (3.28); N 4.36 (4.41). This same batch of single crystals were then returned to a glass vial that was kept in a humid environment for 24 h, and single crystal X-ray diffraction showed that **3** had reformed and the crystal quality had improved. The experiment was repeated on the same crystals three times with the same results.

Powder X-ray Diffraction. To test for phase purity of the crystalline products, we collected samples for compounds **1**−**5** from the walls of the solvothermal tubes, washed the samples with

dx.doi.org/10.1021/ic501581c | Inorg. Chem. 2014, 53, 9932−9945

Table 1. Crystallographic Data

	1	2	3	3*	4	5
formula	$C_{30}H_{23.82}CaN_2O_{9.91}$	$C_{30}H_{24}CaN_2O_{12}$	$C_{30}H_{28.04}N_2O_{12.02}Sr$	$C_{30}H_{28.10}N_2O_{12.05}Sr$	$C_{30}H_{22}N_2O_9Sr$	$C_{30}H_{22}N_2O_{11}Sr$
fw, g mol^{-1}	610.97	644.59	696.57	697.03	642.11	674.11
crystal system	tetragonal	monoclinic	tetragonal	tetragonal	tetragonal	orthorhombic
space group	$P4_32_12$	$C2$	$P4_12_12$	$P4_32_12$	$P4_12_12$	$P2_12_12_1$
T, K	296(2)	100(2)	100(2)	100(2)	100(2)	100(2)
a, Å	20.8348(16)	15.585(4)	19.868(3)	19.9415(9)	19.030(5)	7.0910(9)
b, Å	20.8348(16)	21.919(5)	19.868(3)	19.9415(9)	19.030(5)	14.1845(18)
c, Å	14.064(2)	8.214(2)	14.975(4)	14.9995(13)	14.797(7)	26.618(3)
β, deg		103.410(4)				
V, Å^3	6104.9(12)	2729.6(11)	5911.0(18)	5964.8(7)	5359(4)	2677.3(6)
Z	8	4	8	8	8	4
R_1 ($I > 2\sigma(I)$)[a]	0.0564	0.0438	0.0538	0.0325	0.1329	0.0304
wR_2 ($I > 2\sigma(I)$)[b]	0.1428	0.0971	0.1118	0.0841	0.3251	0.0646
Flack parameter	0.01(5)	−0.01(3)	−0.015(11)	−0.018(2)	0.072(13)	−0.007(4)

[a] $R1 = \sum ||F_o| - |F_c|| / \sum |F_o|$. [b] $wR2 = \{\sum [w(F_o^2 - F_c^2)^2] / \sum [w(F_o^2)^2]\}^{1/2}$.

methanol, and ground them in air. For the dehydrated versions, single crystals were kept under vacuum overnight and then ground. All measurements were performed on a Rigaku Ultima 4 instrument using Cu Kα radiation at a scan rate of 1°/min between 5 and 30° 2θ with a step size of 0.02° 2θ. Powder patterns were analyzed using Microsoft Excel and were compared to the powder patterns predicted by Mercury based on the single crystal data. These powder patterns are shown in the Supporting Information, Figures S1−S8, and demonstrate phase purity for **2**−**5**. Compound **1** decomposed rapidly in air; the powder spectrum did not match the single crystal data.

Crystallographic Studies. For all complexes, X-ray diffraction intensity data were measured at 100(2) K except for compound **1** (296 K), using a Bruker SMART APEX diffractometer (Mo Kα radiation, λ = 0.71073 Å). The raw area detector data frames were reduced with the SAINT+ program. Direct methods structure solution, difference Fourier calculations, and full-matrix least-squares refinement against F^2 were performed with SHELXS/L implemented in OLEX2. Non-hydrogen atoms were refined with anisotropic displacement parameters. Hydrogen atoms bonded to carbon were placed in geometrically idealized positions and included as riding atoms. For compounds **1**−**5** crystal enantiopurity and the "S" configuration (except 3* where it is "R") of the chiral carbon (C13 in all structures) were established by the absolute structure (Flack) parameters of 0 (within experimental error) derived from the X-ray data sets. For compound **1**, the data crystal was mounted inside a thin-walled glass capillary along with a drop of the mother liquor. Previous studies indicated some decomposition of the crystals in air. Attempts to cool crystals in a nitrogen cold stream resulted in loss of crystallinity accompanied by clouding of the crystals and broadening of the diffraction maxima. Details of data collection are given in Table 1, and the solution and refinement of structures are detailed in the Supporting Information.

RESULTS

Synthesis. Single crystals of $[Ca(\mathbf{L}_{ala})_2(H_2O)]\cdot(H_2O)$ (**1**), $[Ca(\mathbf{L}_{ser})_2]\cdot(H_2O)_2$ (**2**), $[Sr(\mathbf{L}_{ala})_2(H_2O)]\cdot(H_2O)_3$ (**3**), $[Sr(\mathbf{L}_{ala}{*})_2(H_2O)]\cdot(H_2O)_3$ (**3***), and $[Sr(\mathbf{L}_{ser})_2(H_2O)]$ (**5**) were synthesized via solvothermal methods by combining the potassium salt of each respective ligand and the appropriate alkaline metal nitrate (2:1 molar ratio) in a mixed solvent system containing mixture of either methanol/water or isopropyl alcohol/water. The sealed tubes were heated at 120 °C in an oil bath with the crystals growing slowly just above the solvent line of the hot tube.

Compound **3** undergoes a single-crystal to single-crystal transformation when placed under vacuum to form compound **4**, $[Sr(\mathbf{L}_{ala})_2(H_2O)]$, where the interstitial waters in **3** are removed, but the coordinated water molecule remains. Placing crystals of **4** in a humid atmosphere leads to the reformation of crystalline **3**, a process that can be repeated at least three times. Monitoring the crystals at each step by single crystal X-ray diffraction demonstrates that single crystallinity is retained in this process.

Structure Descriptions. Compound **1**, $[Ca(\mathbf{L}_{ala})_2(H_2O)]\cdot(H_2O)$, is composed of calcium cations bridged by $\mathbf{L}_{ala}^-$ ligands into a chiral helical rod SBU that is interdigitated with adjacent parallel rods by the supramolecular $\pi\cdots\pi$ stacking of the naphthalimide rings to generate a 3D SMOF structure. The coordination number of the calcium cation is 7, and the irregular polyhedron most closely resembles a capped octahedron. There are two nonequivalent ligands, and each has different a coordination mode (Figure 1). One carboxylate

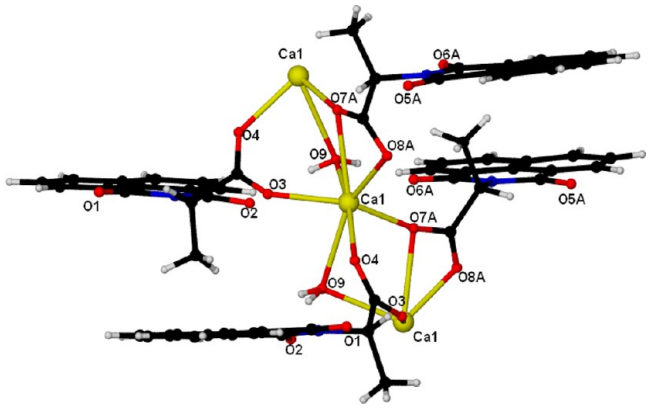

Figure 1. Ca^{2+} coordination environment of $[Ca(\mathbf{L}_{ala})_2(H_2O)]\cdot(H_2O)$ (**1**).

adopts a μ−κ^1:κ^2 bonding mode (this ligand is disordered over two sites, but only one version is shown), while the other adopts a μ−κ^1:κ^1 bonding mode, thus filling five of the seven coordination sites. Another key difference between the two ligands is the orientation of the methyl groups at the chiral centers, which are oriented in opposite directions with respect to the crystallographic c axis. The last two metal sites are occupied by a bridging water molecule generating the edge shared polyhedra that make up the helical rod SBU. The homochiral M helices created by the bridged calcium cations have a pitch of 14.06 Å (Figure 2). There are two types of $\pi\cdots\pi$

dx.doi.org/10.1021/ic501581c | Inorg. Chem. 2014, 53, 9932−9945

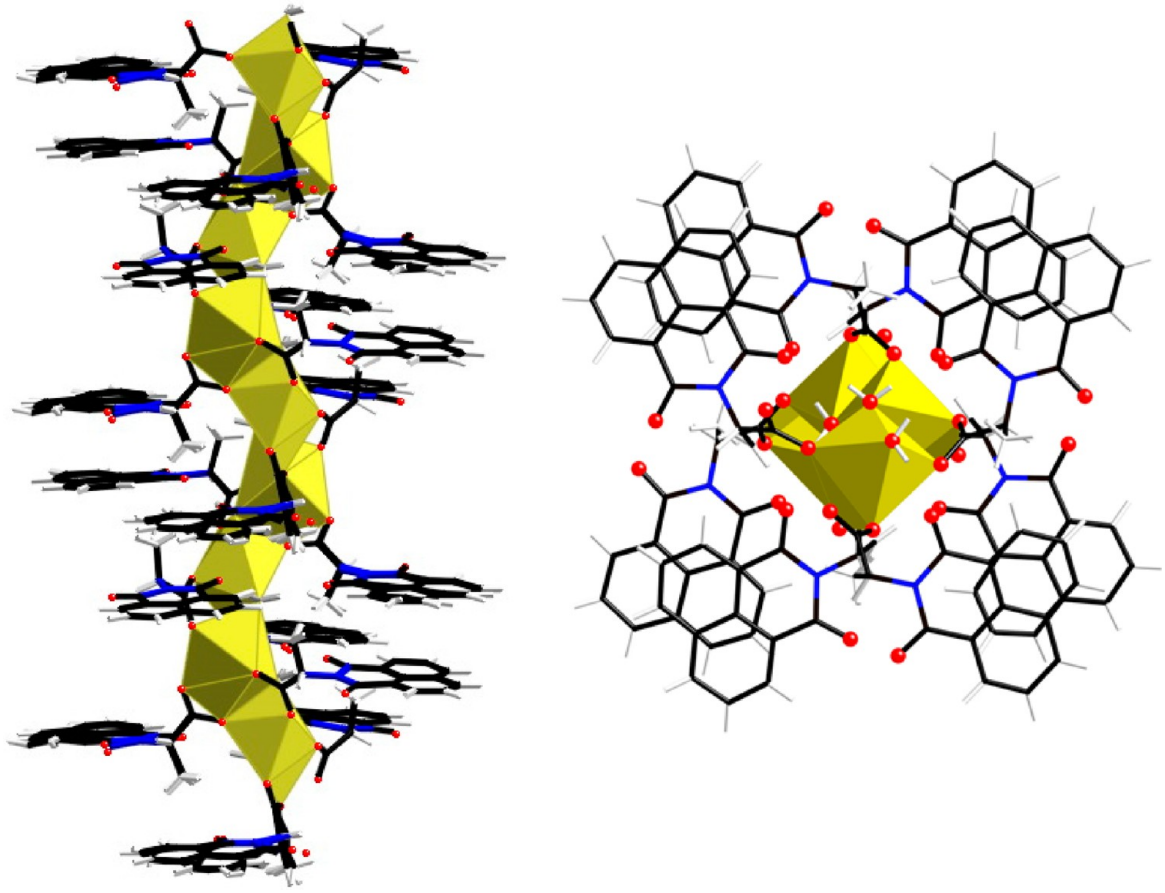

Figure 2. (Left) Side view of the helical rod formed for **1** by edge shared calcium polyhedra and (right) a top-down view of the helices showing the naphthalimide overlap of intra-rod $\pi\cdots\pi$ stacking.

Table 2. $\pi\cdots\pi$ Stacking Parameters

	compd	type of stacking	center-to-center distance(Å)	dipole angle (deg)[a]	plane angle (deg)	av distance (Å)	χ (Å)[b]
1	$[Ca(\mathbf{L}_{ala})_2(H_2O)]\cdot(H_2O)$	intra-rod	3.77	53	1.7	3.50	1.42
		inter-rod	3.62	129	0.5	3.48	0.99
		inter-rod	3.67	115	3.8	3.51	1.06
2	$[Ca(\mathbf{L}_{ser})_2]\cdot(H_2O)_2$	inter-rod	4.37	137	27	4.04	1.69
		inter-rod	4.17	130	26	3.93	1.39
3	$[Sr(\mathbf{L}_{ala})_2(H_2O)]\cdot(H_2O)_3$	inter-rod	4.46	91	8.6	3.48	2.79
		inter-rod	3.57	127	9.7	3.48	0.73
		inter-rod	3.54	64	9.3	3.51	0.47
4	$[Sr(\mathbf{L}_{ala})_2(H_2O)]$	inter-rod	4.46	71	1.2	3.31	2.98
		inter-rod	3.51	70	6.9	3.50	0.23
		inter-rod	4.00	52	10.7	3.55	1.84
5	$[Sr(\mathbf{L}_{ser})_2(H_2O)]$	inter-rod	4.00	160	19.8	3.46	1.96
		inter-rod	4.42	176	19.8	3.48	2.68

[a]Relative rotation of the rings (180° is the head-to-tail arrangement). [b]Slippage parameter, the third side of the right triangle formed with the average perpendicular distance between the two rings and the line between the two central carbon atoms of the rings.

stacking in which the naphthalimide rings are involved: intra-rod $\pi\cdots\pi$ stacking, where ligands with opposing methyl orientation from the same rod stack together, and inter-rod $\pi\cdots\pi$ stacking where ligands from adjacent rods interact with one another to generate the 3D SMOF structure. All of the ligands are involved in both types of $\pi\cdots\pi$ stacking, creating pairs of 1,8-naphthalimide rings that interdigitated with pairs from an adjacent rod. The metrics used to evaluate the $\pi\cdots\pi$ stacking are listed in Table 2. The π-stacked pairs of naphthalimide rings of **1** are oriented in a "square" arrangement, Figure 2 (right), so that each rod interacts with four adjacent rods, generating a 3D network with square shaped channels (Figure 3). These channels are occupied by disordered water molecules.

Compound **2**, $[Ca(\mathbf{L}_{ser})_2]\cdot(H_2O)_2$, contains calcium cations bridged by $\mathbf{L}_{ser}^-$ ligands into a homochiral rod SBU that interacts with adjacent parallel rods through supramolecular interactions of the naphthalimide rings. The eight coordinate calcium cations are bridged through μ–κ^1:κ^2 carboxylates that occupy six of the coordination sites (Figure 4). The remaining

dx.doi.org/10.1021/ic501581c | Inorg. Chem. 2014, 53, 9932–9945

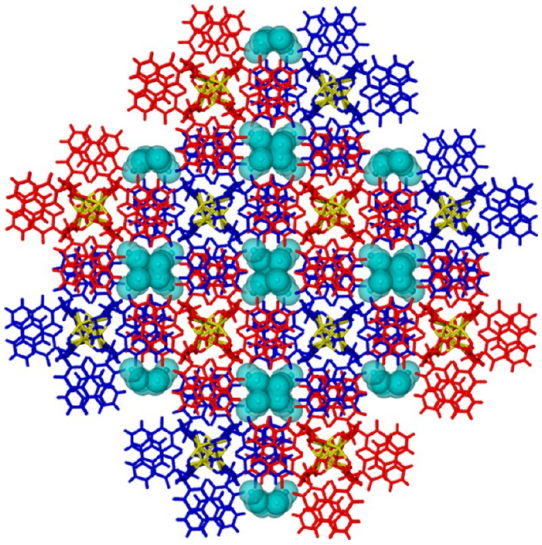

Figure 3. Top-down view of the 3D supramolecular structure of compound **1**; (yellow) calcium cations, (red and blue) adjacent helices, and (teal) disordered interstitial water molecules.

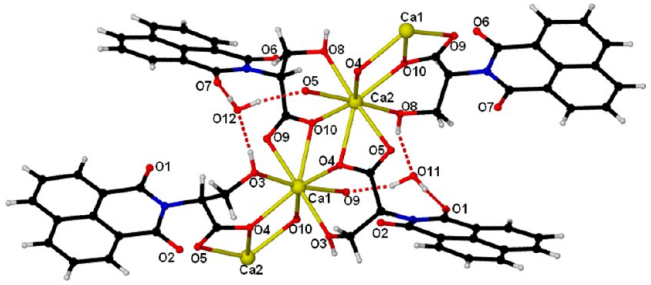

Figure 4. Ca^{2+} coordination environment of $[Ca(\mathbf{L}_{ser})_2]\cdot(H_2O)_2$ (**2**).

sites are occupied by the alcohol group, an additional donor group designed into the ligand, which chelates the calcium atoms generating 6-member rings. The homochiral zigzag rods created by bridged calcium cations have a pitch of 8.21 Å (Figure 5). There are interstitial water molecules present that are hydrogen bonded to the alcohol, the naphthalimide carbonyl and one of the bridging carboxylates, all within the same SBU. The naphthalimide rings in compound **2** are oriented in a rectangular shape (Figure 5, right) with two pairs of naphthalimide rings interdigitating with two pairs on adjacent rods generating a two-dimensional structure of layered sheets (Figure 6). There are no strong supramolecular interactions between the sheets. The $\pi\cdots\pi$ stacking metrics for compound **2** are listed in Table 2.

Compound **3**, $[Sr(\mathbf{L}_{ala})_2(H_2O)]\cdot(H_2O)_3$, contains strontium cations bridged by $\mathbf{L}_{ala}^-$ ligands into a homochiral helical rod SBU that interacts with adjacent parallel rods through supramolecular interactions of the naphthalimide rings. Each of the strontium cations is eight-coordinate. Six of the eight coordination sites are occupied by bridging $\mu{-}\kappa^1{:}\kappa^2$ carboxylates from four different ligands. While the two nonequivalent ligands share the same coordination mode, they are distinct in that one has a coordinated naphthalimide carbonyl oxygen that forms a 7-membered chelate ring while the other does not. The ligand without the second mode of coordination is disordered over two positions; only one is shown. The last coordinate site is occupied by a water molecule that is involved in hydrogen bonds to the carboxylate O8A and to the naphthalimide carbonyl O6A from a different ligand (Figure 7). The *P* helix created by edge-shared strontium polyhedra has a pitch of 14.98 Å (Figure 8, left). Each of the helical rods interacts with four adjacent rods through strong $\pi\cdots\pi$ stacking interactions, generating rectangular channels with a pore size of 1.9 × 7.7 Å that are occupied by disordered water molecules (Figure 9). The $\pi\cdots\pi$ stacking metrics for compound **3** are listed in Table 2.

The structure of compound **3***, formed with the ligand R-isomer, $\mathbf{L}_{ala}{}^{*-}$, is the same as **3**, but it is in the enantiomeric space group. As shown in Figure 8 (right), the helical rod has the opposite, *M*-helicity.

Compound **3** undergoes a single-crystal to single-crystal transformation when **3** is left under vacuum to form $[Sr(\mathbf{L}_{ala})_2(H_2O)]$ (**4**), during which all of the interstitial water is removed. The overall structure about strontium and the SBU rods for compound **4** are similar to **3** (Figure 10), but the unit cell volume has been reduced by about 9%, mostly along the crystallographic *a* and *b* axes. Figure 11 shows that the once open channels of **3** are now gone, generating a closed form. There are surprisingly large differences in the $\pi\cdots\pi$ stacking metrics, as listed in Table 2.

Compound **5**, $[Sr(\mathbf{L}_{ser})_2(H_2O)]$, contains strontium cations bridged by $\mathbf{L}_{ser}^-$ ligands into a homochiral rod SBU that interacts with adjacent parallel rods through supramolecular interactions of the naphthalimide rings. The strontium cations are nine-coordinate and bridged by $\mu{-}\kappa^2$ carboxylates from four different ligands. This monodentate carboxylate coordination mode leaves room for the alcohol group of both ligands to coordinate forming 6-membered chelate rings. In addition, for one of the two ligands, a naphthalimide carbonyl oxygen bonds and forms a [3.2.2] bicycle with the strontium cation through the carboxylate, the alcohol, and one of the carbonyls of the naphthalimide ring (Figure 12). Another difference from compound **3** is that the water molecule bridges strontium cations. Because there are now three bridging oxygen atoms between each cation, this chiral rod SBU is composed of face-sharing strontium polyhedra (Figure 13). The *M* helix created by the bridged strontium cations has a pitch of 7.09 Å. Each of the rods interacts with four adjacent rods through $\pi\cdots\pi$ stacking of the naphthalimide rings, but no channels form in this compound due to the offset packing (Figure 14). The $\pi\cdots\pi$ stacking metrics for compound **5** are listed in Table 2.

Infrared Spectroscopy. Infrared spectroscopy, coupled with the preparation of isotopomers, was employed to enable us to better understand the role of both the interstitial and coordinated waters during the "breathing mechanism" of the interconversion of $[Sr(\mathbf{L}_{ala})_2(H_2O)]\cdot(H_2O)_3$ (**3**) and $[Sr(\mathbf{L}_{ala})_2(H_2O)]$ (**4**). To eliminate the impact of atmospheric moisture, we ground samples in a drybox with nujol oil, and the sample chamber of the FT-IR instrument had a continuous flow of nitrogen. The spectra for compound **3** and $[Sr(\mathbf{L}_{ala})_2(D_2O)]\cdot(D_2O)_3$, $\mathbf{3d}_8$ (prepared using D_2O as the solvent in the reaction), are shown in Figure 15a,d. For **3** (Figure 15a), an O−H stretching vibration is located at 3520 cm^{-1}, and for $\mathbf{3d}_8$ (Figure 15d), an O−D stretching vibration is located at 2600 cm^{-1}. The broad peak and two small humps just below 3000 cm^{-1} and the two sharp peaks below 2400 cm^{-1} are due to the nujol oil. Spectra run on crystals of both compounds exposed to vacuum, now the dehydrated forms **4** and $\mathbf{4d}_2$ (Figure 15b,e), show similar H_2O and D_2O peaks, respectively. When **4** is rehydrated with D_2O vapor for 24 h, compound $\mathbf{3d}_8$ forms; the IR spectrum (Figure 15c) shows only a D_2O peak and little or none of the H_2O peak. When $\mathbf{4d}_2$ is introduced to H_2O vapor,

dx.doi.org/10.1021/ic501581c | Inorg. Chem. 2014, 53, 9932−9945

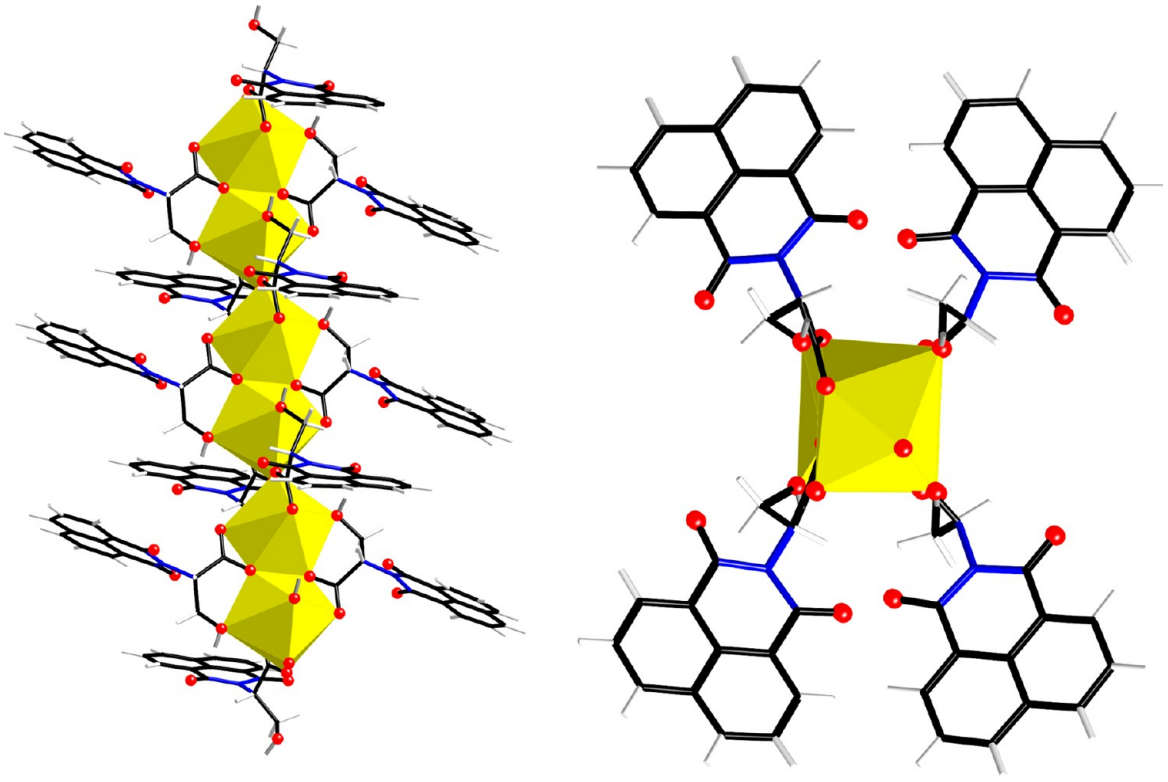

Figure 5. (Left) Side view of the zigzag rod in **2** formed by edge shared calcium polyhedra and (right) a top-down view of the rod.

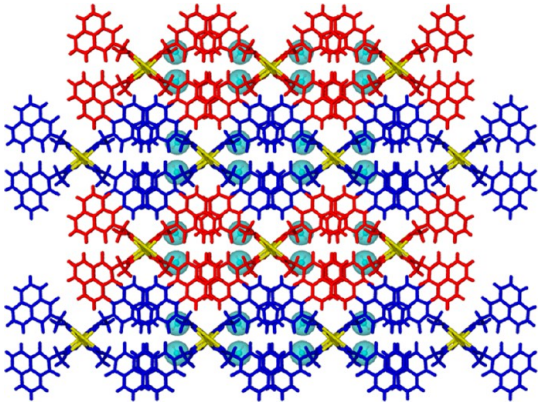

Figure 6. Top-down view of the supramolecular structure of compound **2** with calcium cations highlighted in yellow and rods involved in π stacking are the same color. The sheets of homochiral rods composed of interdigitated naphthalimide rings extend from left to right, and adjacent sheets are different colors. The hydrogen bonded water molecules are colored teal.

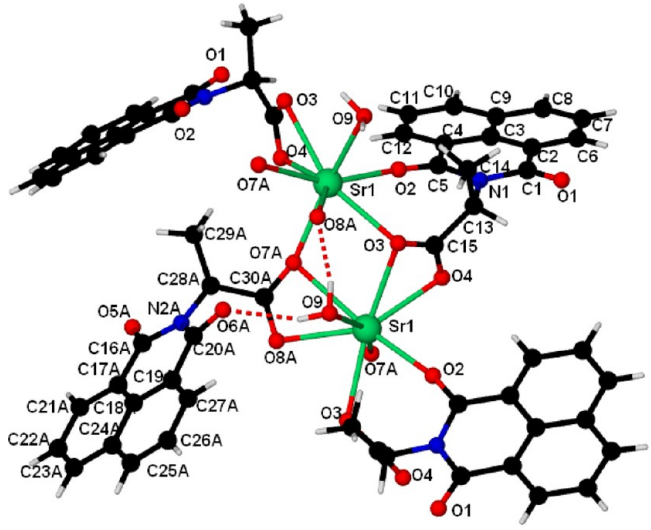

Figure 7. Sr^{2+} coordination environment of $[Sr(\mathbf{L}_{ala})_2(H_2O)]\cdot(H_2O)_3$ (**3**).

compound **3** forms; the IR spectrum (Figure 15f) shows only the H_2O peak and little or none of the D_2O peak. The coordinated water cannot be distinguished from the interstitial water in any of these spectra.

Nuclear Magnetic Resonance (NMR). Solid-state nuclear magnetic resonance experiments were performed on compounds **3** and **4** to investigate the use of these methods on the single-crystal to single-crystal transformation. The ^{1}H NMR experiments had poor resolution, but some information could still be learned. Fortunately, the ^{13}C NMR spectra have well-resolved resonances, and assignments can be made when coupled with frequency-switched Lee−Goldburg heteronuclear correlation (FSLG HETCOR) spectroscopy (Figure 16). The resonances at 15 ppm in the ^{13}C NMR spectra are assigned to the methyl group and correlate strongly with the resonance at 1.5 ppm in the ^{1}H NMR spectra. The methine carbon has a distinguishing resonance at 60 ppm in the ^{13}C NMR spectra that correlates strongly with the resonance at 4.5 ppm in the ^{1}H NMR spectra. The large resonances around 140 ppm are assigned to the aromatic carbons, which correlate to the 7 ppm range in the ^{1}H NMR spectra. The naphthalimide carbonyl resonances are located at 160 ppm, and the carboxylate carbonyl resonances are at 175 ppm. Even though **3** and **4** share the same assignments, they can be clearly differentiated by their ^{13}C NMR spectra. ^{1}H NMR experiments on compounds **3** and

dx.doi.org/10.1021/ic501581c | Inorg. Chem. 2014, 53, 9932−9945

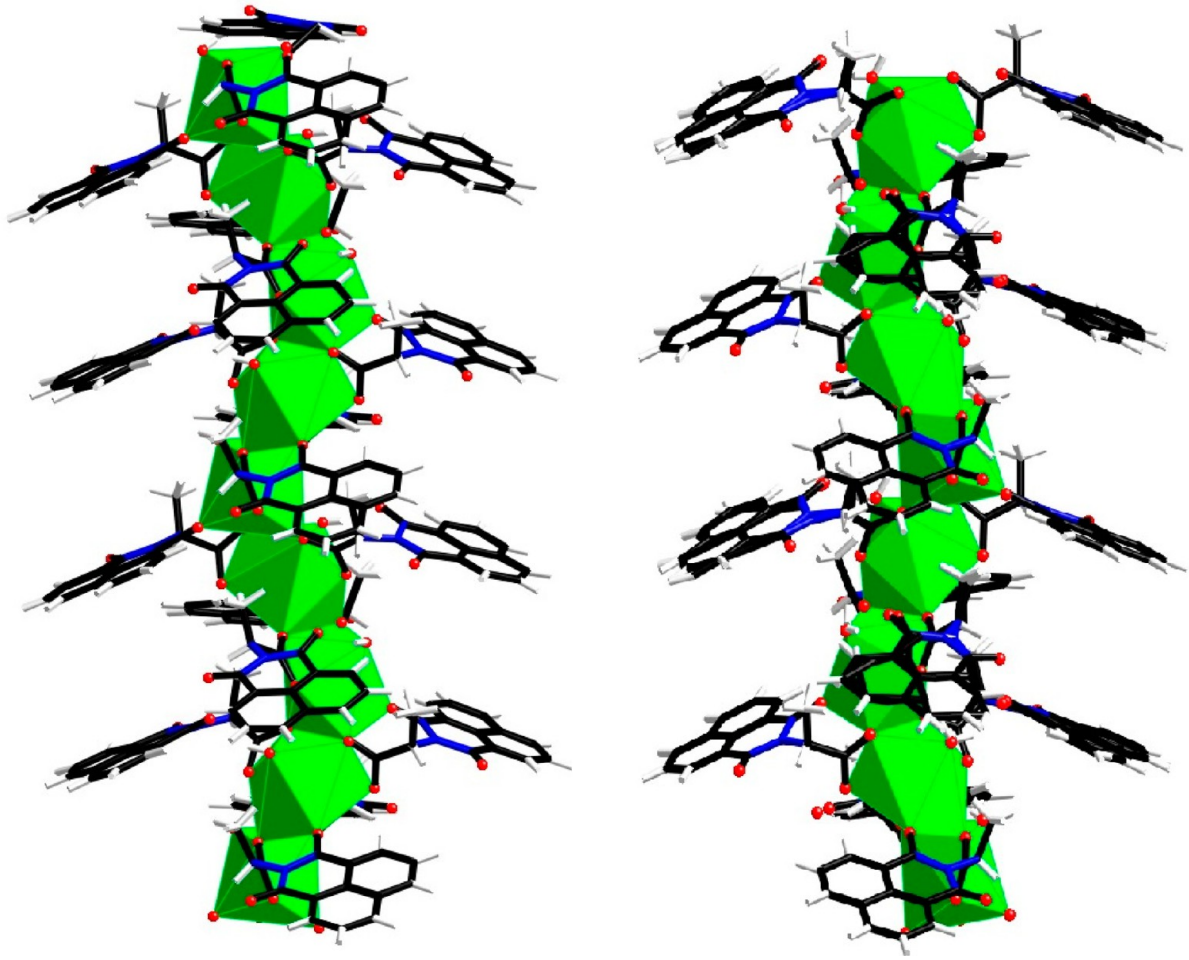

Figure 8. Chiral rods in (left) **3** and (right) **3*** formed by edge shared strontium polyhedra generating *P* and *M* helices, respectively.

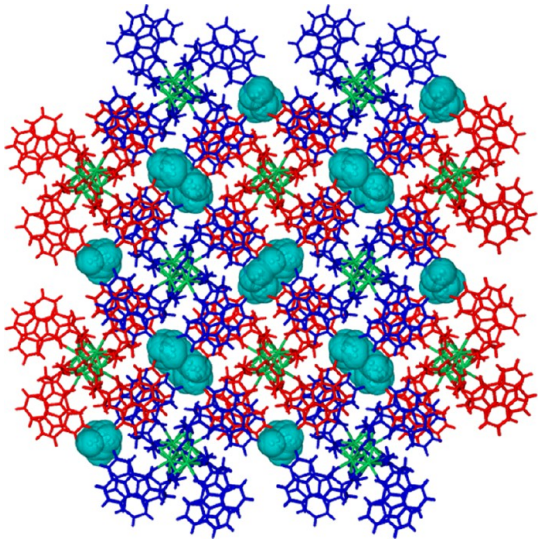

Figure 9. A top-down view of the 3D supramolecular structure of compound **3**; (green) strontium cations, (red and blue) adjacent helices, and (teal) disordered interstitial water molecules.

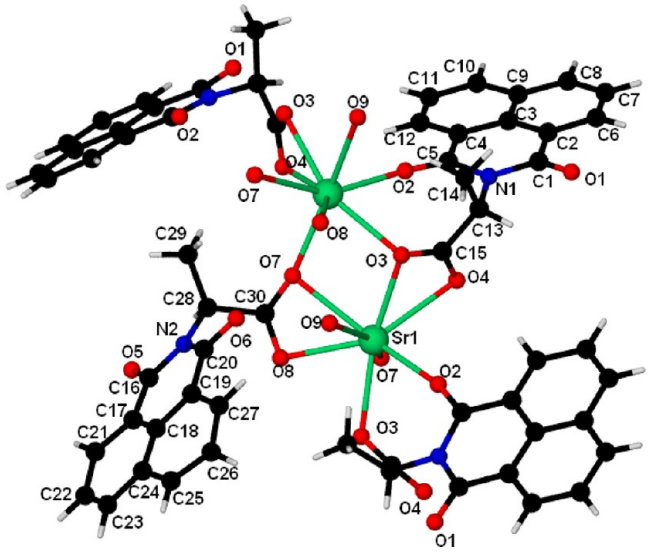

Figure 10. Sr^{2+} coordination environment of $Sr(L_{ala})_2(H_2O)$ (**4**).

4 show nearly identical spectra, but **3** has a much larger integration at 4.5 ppm than **4** does. The resonance at 4.5 ppm has two components; one from the methine hydrogen of the ligand, as confirmed by HETCOR experiments, and the other from the water contribution, which has much less integration for compound **4**.

This assignment of the water resonance was confirmed by ^2H NMR experiments. The ^2H NMR experiments were carried out on crystals prepared using deuterated solvents D_2O and D_3COD to yield the compound $\mathbf{3d_8}$. Initial ^2H NMR

dx.doi.org/10.1021/ic501581c | Inorg. Chem. 2014, 53, 9932−9945

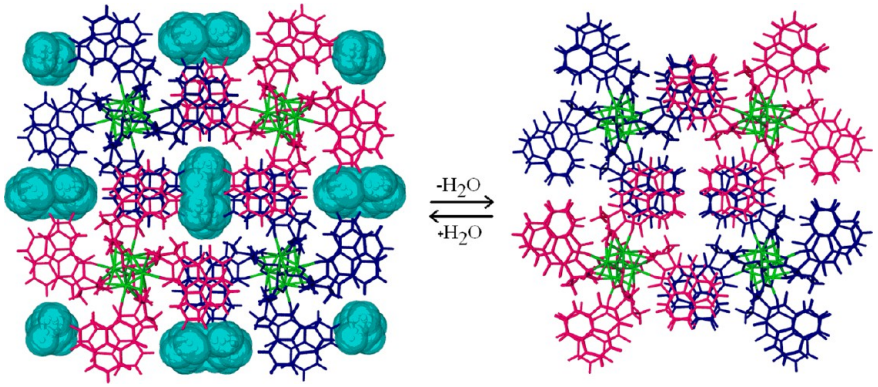

Figure 11. View showing how the channels of compound **3** (left) close in **4** (right) along the crystallographic *a* and *b* axes; (green) strontium cations, (pink and blue) adjacent helices, and (teal) disordered interstitial water molecules.

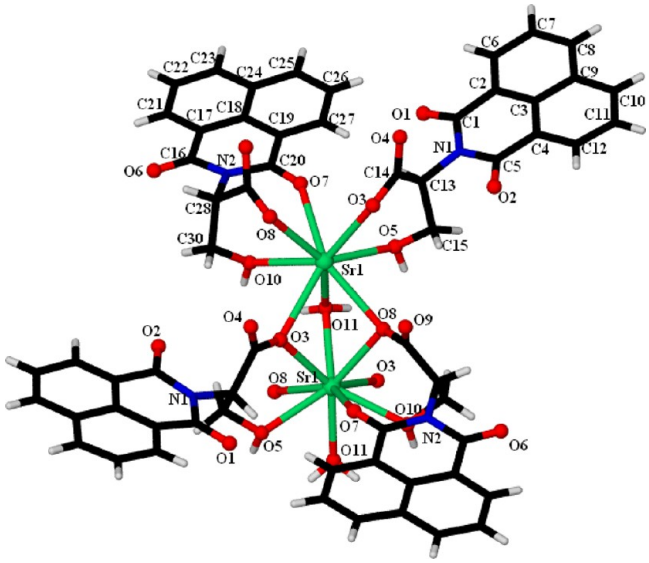

Figure 12. Sr^{2+} coordination environment of $[Sr(\mathbf{L}_{ser})_2(H_2O)]$ (**5**).

experiments were measured on as-prepared crystals that were not vacuum-dried, because drying also removes the interstitial waters of **3**. The fast spinning spectra showed a sharp resonance and a small broad resonance that was apparent after deconvolution (Figure 17a). As the spin rate decreased, the two components split more, and it is more obvious (Figure 17b) that there is a sharp and weaker broad component (Pake pattern). Because of the sharpness of the dominant resonance, indicating that this species is in the fast motion limit in the solid-state,[14] the sharp component was attributed to adsorbed water on the crystals, and the broad component was attributed to compound **3**. To confirm this assignment, we removed the adsorbed water by drying and thus dehydrating compound $\mathbf{3d}_8$ and rehydrating the resulting compound $\mathbf{4d}_2$ in the presence of D_2O vapor, restoring compound $\mathbf{3d}_8$, but now with no adsorbed water. Spectra of this sample (Figure 17c,d) show only the broad peak that had been deconvoluted from the original spectrum of the as-prepared crystals, confirmed by chemical shift and similar half height widths of 140 Hz. Due to the broadness of the resonance, the interstitial water was found to be indistinguishable from the coordinated water by ^{2}H NMR spectroscopy, but the chemical shift assignment made from the ^{1}H spectra around 4.5 ppm was confirmed.

Thermal Analysis. Thermal gravimetric analyses of compounds **1**–**5** under a steady stream of dry air are shown in Figure 18. Upon heating, compound **1** experiences a weight loss between 51 and 181 °C corresponding to the loss of coordinated and interstitial water from the compound (7.5%, calcd 5.6%). Compound **1** remains stable upon further heating until it reaches the decomposition point of 357 °C, well beyond the decomposition point of the protonated ligand, $H\mathbf{L}_{ala}$. At this temperature the solid begins to froth, so the experiment was terminated. Compound **2** undergoes a similar weight loss between 64 and 139 °C corresponding to the loss of interstitial water (6.4%, calcd 5.6%). Compound **2** remains stable until it reaches the decomposition point of 249 °C. Compound **3** shows a gradual weight loss between 35 and 197 °C corresponding to the loss of coordinated and interstitial water (9.0%, calcd 10.3%) and remains stable until decomposition at 305 °C. Thermal analysis of compound **5** shows the loss of coordinated water between 104 and 186 °C (2.6%, calcd 2.6%) and remains stable until decomposition at 247 °C.

Rehydration experiments were performed with all compounds by switching to ambient air. In the cases of compounds **2** and **5**, when crystals were heated well above the dehydration point followed by cooling in air, water was reincorporated over a period of ca. 18 h, resulting in the compounds regaining the lost weight (Figure 19). These solids lost single crystallinity in this process but were shown to retain crystallinity at the end of the rehydration by powder X-ray diffraction (PXRD; see Supporting Information). In similar experiments, compound **3** does not rehydrate for 1 week. In this case, PXRD experiments on the heated and dehydrated solid of **3** show loss of crystallinity.

As outlined in the NMR section, ^{2}H NMR experiments indicated that the as-prepared crystals of **3** contained some adsorbed water. To test for the presence of this adsorbed water, we carried out TGA analyses on the as-prepared compound $\mathbf{3d}_8$ that had undergone the brief air drying protocol used in the initial NMR experiment and another batch of crystals that had been dried and rehydrated with D_2O ($\mathbf{3d}_8 \rightarrow \mathbf{4d}_2 \rightarrow \mathbf{3d}_8$). As shown in Figure 20, the weight loss of the two samples was different, and the weight difference between the two was 0.56% (about 0.3 water molecules per strontium cation).

Fluorescence Analysis. Compounds **1**–**3** and **5** exhibit substantial solid-state fluorescence originating from the naphthalimide chromophore in the ligand, and their spectra are shown in Figure 21. In the case of the $\mathbf{L}_{ala}^-$ adducts of the group 2 metals (**1** and **3**), the fluorescence maximum is red-

dx.doi.org/10.1021/ic501581c | Inorg. Chem. 2014, 53, 9932–9945

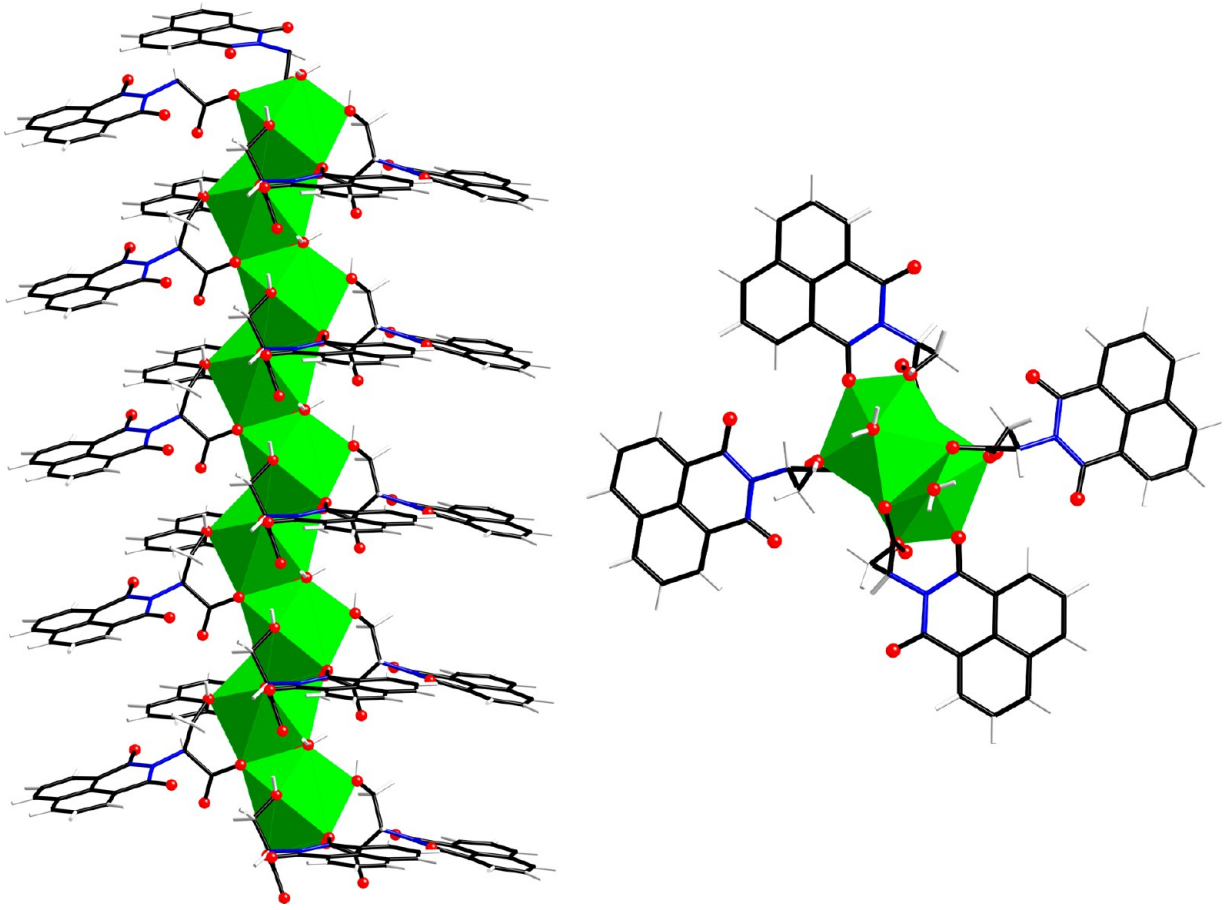

Figure 13. (Left) Side view for **5** of the chiral rod formed by face-shared strontium polyhedra and a (right) top-down view of the rod.

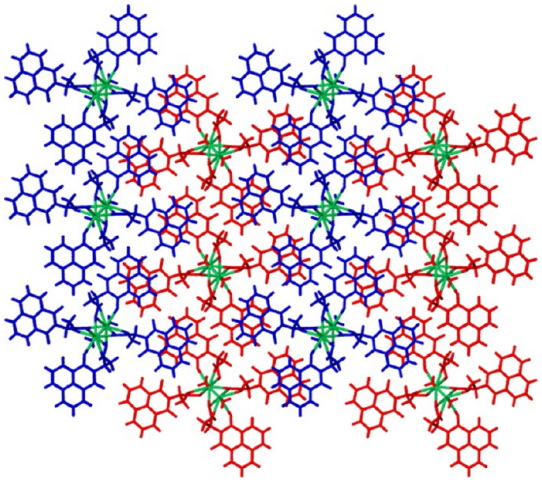

Figure 14. A top-down view along the crystallographic *a* axis of the 3D supramolecular structure of compound **5**; (green) strontium cations and (blue and red) adjacent helices.

shifted with respect to the ligand, and in the case of L_{ser}^- adducts of the group 2 metals (**2** and **5**), the fluorescence maximum is blue-shifted with respect to the ligand.

DISCUSSION

We have prepared a series of compounds from two alkaline earth metals (Ca^{2+} and Sr^{2+}) and L_{ala}^- ($L_{ala}{}^{*-}$) and L_{ser}^- (Scheme 1) ligands, designed for the preparation of enantiopure, chiral supramolecular MOFs (SMOFs). Similar to complexes of these ligands with group 1 metals, a consistent structural motif is formed where homochiral rod-shaped SBUs dominate the topology and $\pi\cdots\pi$ stacking between 1,8-naphthalimide rings link adjacent rod SBUs with supramolecular interactions. While the rod structural motif is the same in all compounds, there are important differences, including how the cations are bridged by carboxylate groups and solvent, the orientation and overlap of the naphthalimide rings and whether the compounds are porous. The coordination number of the cations that make up the rod-shaped SBU range from seven-coordinate (**1**) to nine-coordinate (**5**), whereas the other compounds (**2**, **3**, **3***) are eight-coordinate. All of the SBUs are homochiral and consist of either edge-shared polyhedra (**1**–**4**) or the unusual face-shared polyhedra (**5**). Very few MOFs containing homochiral rod SBUs have been reported previously.[15] As expected, the structures of **3** and **3***, formed from enantiomeric forms of the same ligand, are the same, but the rods have opposite helicity.

The most prominent structural feature of this work, especially when coupled with our previous paper on group 1 metals with the same ligands, is the consistent formation of rod SBUs, rods that are necessarily homochiral because of building the ligands from enantiopure amino acids. The s-block metals generally lack the formation of consistent SBUs as one varies the metals,[12] although it has been pointed out recently that the larger metals of group 1 are likely to form rod structures with anionic oxygen donor ligands.[16] With our ligands containing

dx.doi.org/10.1021/ic501581c | Inorg. Chem. 2014, 53, 9932–9945

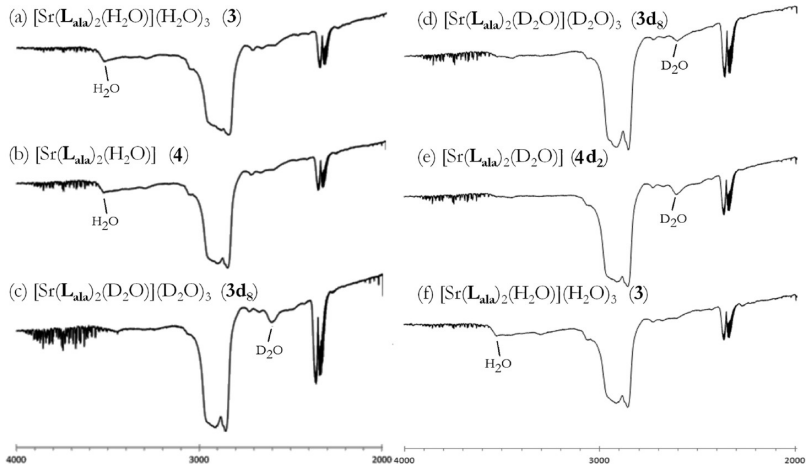

Figure 15. Infrared spectra of Nujol mull of (a) compound **3** which was (b) dehydrated then (c) rehydrated with D_2O. The opposite was done with (d) the perdeutero **3d$_8$** which was (e) dehydrated then (f) rehydrated with H_2O.

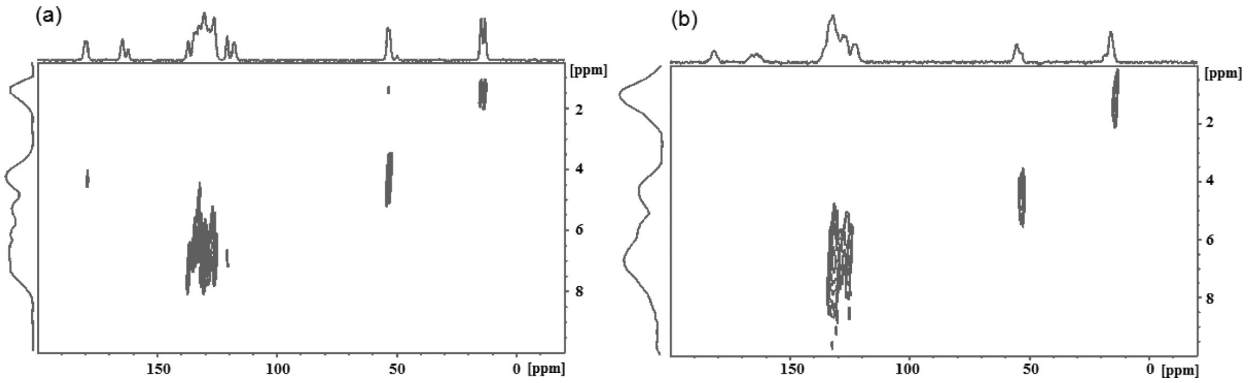

Figure 16. FSLG HETCOR spectra of compounds (a) **3** and (b) **4**.

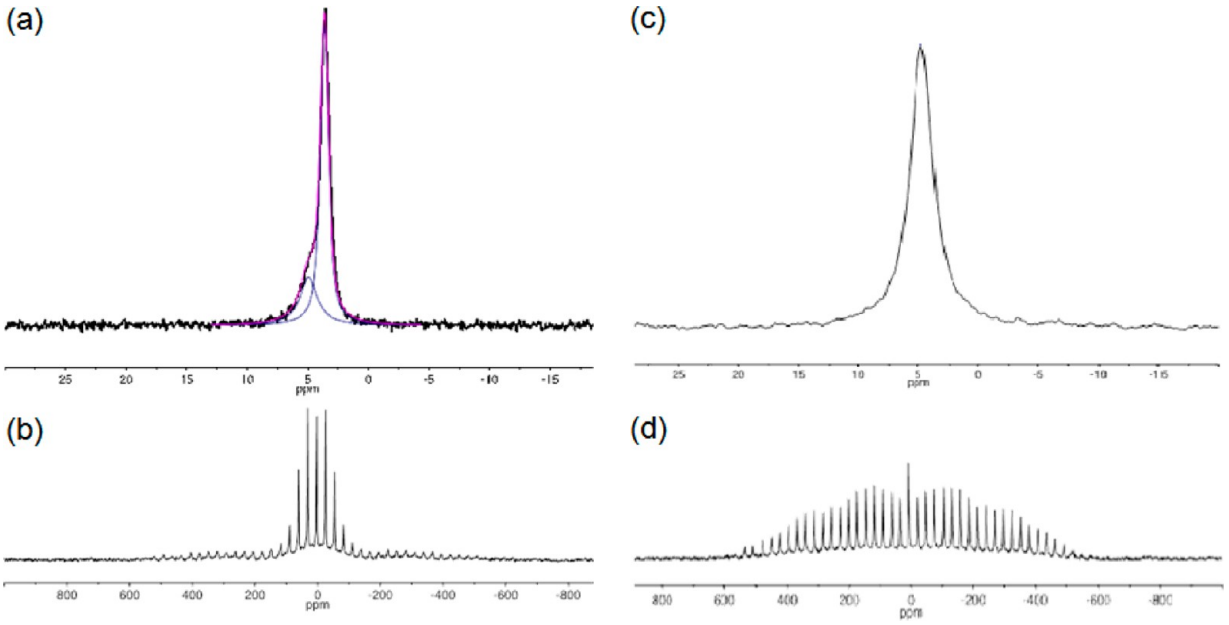

Figure 17. ^{2}H NMR spectra of as-prepared **3d$_8$**: (a) fast spin and (b) slow spin. ^{2}H NMR spectra of **3d$_8$** after dehydrating and rehydrating in the presence of D_2O: (c) fast spin and (d) slow spin.

the large, $\pi\cdots\pi$ stacking naphthalimide group, we consistently observe rods with both group 1 and 2 metals even though the rods are built from a variety of bridging oxygen donor motifs, including cases where the only bridge comes from the solvent. Nevertheless, the rods consistently form. In contrast, transition metal complexes of these ligands do not form rod SBUs.[6,9,10]

dx.doi.org/10.1021/ic501581c | Inorg. Chem. 2014, 53, 9932−9945

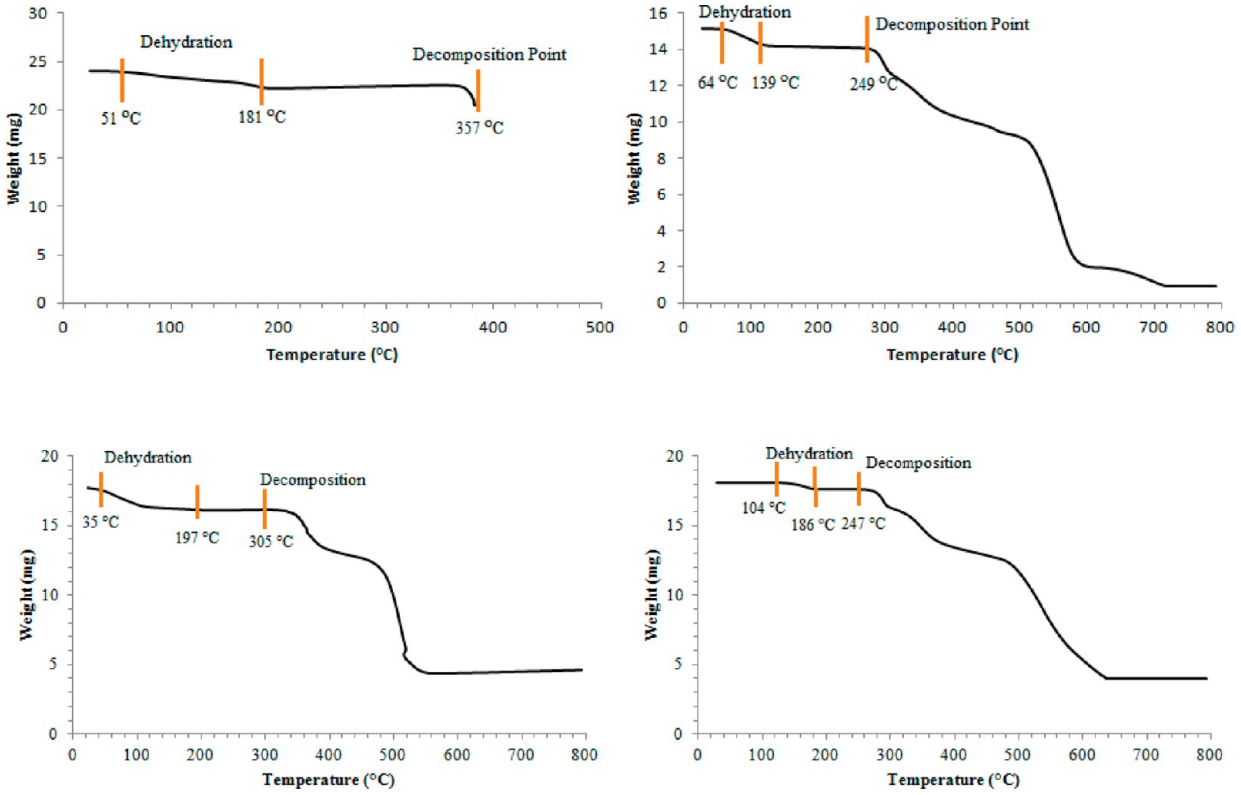

Figure 18. TGA for compounds (top left) **1**, $[Ca(L_{ala})_2(H_2O)]\cdot(H_2O)$; (top right) **2**, $[Ca(L_{ser})_2]\cdot(H_2O)_2$; (bottom left) **3**, $[Sr(L_{ala})_2(H_2O)]\cdot(H_2O)_3$; and (bottom right) **5**, $[Sr(L_{ser})_2(H_2O)]$.

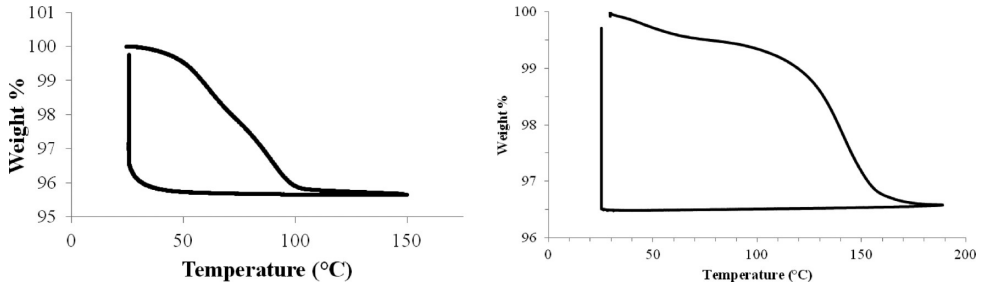

Figure 19. Removal and reuptake of water from (left) compound **2** and (right) compound **5**.

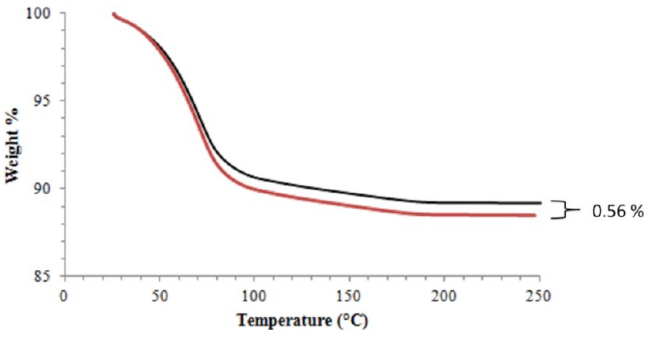

Figure 20. (Red) TGA of as-prepared compound $\mathbf{3d}_8$ and (black) $\mathbf{3d}_8$ after being dehydrated and rehydrated in the presence of D_2O vapor.

In four of the five compounds (**1**, **3**, **4**, and **5**), each rod-shaped SBU is interlocked with four adjacent rods through $\pi\cdots\pi$ stacking in a motif similar to the uninodal 4*c* net if they were covalent connections. In **2**, the naphthalimide rings for one rod are oriented in a position where two pairs of naphthalimide rings interdigitate with two pairs on two adjacent rods resulting in 2D sheets instead of a 3D network. In the case of compounds **1** and **3**, which are complexes with the L_{ala}^- ligand, there are open 1D channels along the crystallographic *c* axis that are occupied by disordered solvent. In the L_{ser}^- ligand compounds **2** and **5**, the introduced alcohol functional group bonds the metal, decreasing ligand flexibility and impacting the structures. In the calcium complex **2**, the alcohol in the ligand occupies the coordination sites occupied by the coordinated solvent in its analogous alanine analog **1**, whereas in the strontium complexes, the presence of an additional oxygen donor serves to increase the coordination number of the cation when compared to the alanine analog **3**. In both complexes with the L_{ser}^- ligand, there are no channels present. Finally, of the eight group 1 complexes reported previously and the group 2 complexes reported here, only compound **1** exhibits intra-rod $\pi\cdots\pi$ stacking.

While compound **1** is unstable in air, compounds **2**–**5** are robust. When compounds **2** and **5** were heated in a dry environment, they lost water as well as single crystallinity, but

dx.doi.org/10.1021/ic501581c | Inorg. Chem. 2014, 53, 9932–9945

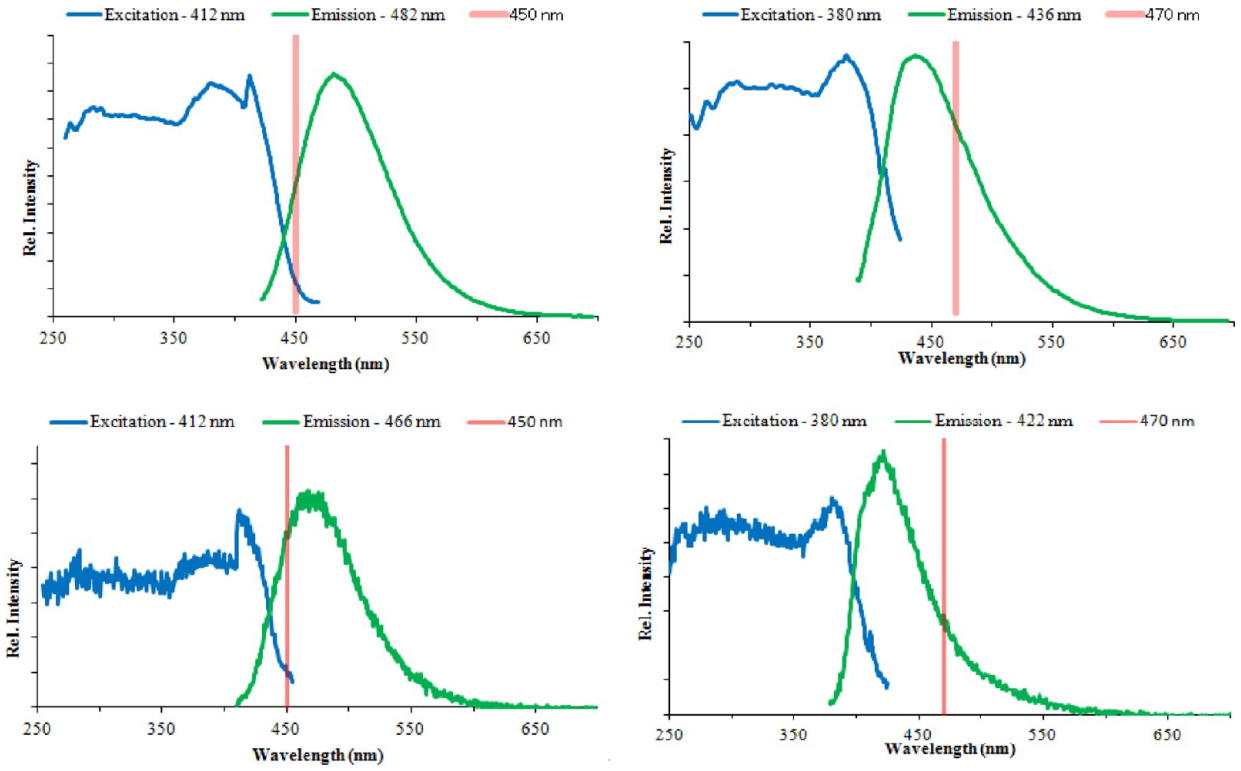

Figure 21. Solid-state fluorescence spectra for compounds (top left) **1**, (top right) **2**, (bottom left) **3**, and (bottom right) **5**; (blue) excitation spectra, (green) emission spectra, and (red) fluorescence maximum of the protonated form of the ligand from each complex HL_{ala} (**1**, **3**) and HL_{ser} (**2**, **5**), respectively.

upon cooling and exposure to atmosphere, the lost water was reincorporated into the structures, as confirmed by TGA and PXRD. The role of the water is different in both compounds, interstitial in **2** and coordinated in **5**. The removal of coordinated and interstitial water could not be differentiated in the TGA of **1**.

In a similar way, compound **3** loses bonded and interstitial waters between 64 and 139 °C (again not differentiated in the TGA), but in this case, the dehydrated solid does not readily rehydrate. In contrast, when exposed to a vacuum, compound **3** loses only interstitial waters but holds coordinated waters, and it retains single crystallinity to form **4**. In this reversible transformation, the pores in compound **3**, which are oriented along the crystallographic *c* axis, are closed by a contraction along the other two crystallographic axes, leaving the unit cell volume of **4** reduced by 9%. The flexibility needed for this process to take place without loss of single crystallinity is imparted into these solids by the inherent flexibility of the $\pi\cdots\pi$ stacking interactions of the naphthalimide rings. As we have discussed before,[9a,17] and again emphasized by the data in Table 2, the rings can rotate and/or slip in the solid state with respect to each other (as measured by the dipole angle and slippage parameter χ, respectively) without any large change in the energy associated with the supramolecular forces. For example, as shown in Figure 22 for two of the interactions, in the transformation of **3** to **4**, the rings rotate (91, 127, and 64° in **3** versus 71, 70, and 52° in **4**) and slip (2.79, 0.73, 0.47 Å in **3** versus 2.98, 0.23, and 1.84 Å in **4**) to accommodate the reversible loss or gain of water. By combining the strong covalent forces of the rod-shaped SBUs with the flexible $\pi\cdots\pi$ stacking of the naphthalimide supramolecular synthon, the structures of the resulting solids can readily adapt to opening or

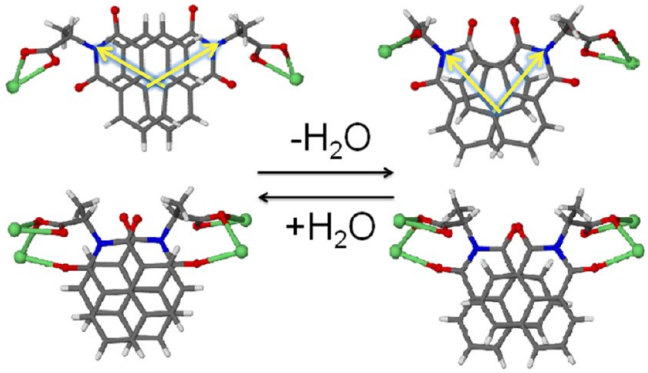

Figure 22. View of two of the $\pi\cdots\pi$ stacking interactions of the naphthalimide rings found in (left) compound **3** and (right) compound **4**. (Top) Dipole vectors between the rings decrease from 127 to 70°, accompanied by a slippage parameter decrease of 0.73 to 0.23 Å. (Bottom) Slippage parameters between the rings increase from 0.47 to 1.84 Å.

closing of the pores while maintaining single crystallinity. This type of "dynamic breathing" for our SMOFs is thus an expected consequence of the design of the system. We note that others have reported the use of hydrogen bonding interactions to prepare complex structures with mixed covalent/supramolecular interactions with interesting properties.[18]

We used the preparation of isotopomers (exchanging D_2O for H_2O), X-ray crystallography, and solid-state IR and ^1H, ^2H, and ^{13}C NMR to more closely investigate the breathing mechanism of compound **3**. Single-crystal X-ray diffraction shows that after exposing dehydrated **4** to D_2O for 24 h the channels reopen and fill with disordered solvent, analogous to the experiments described above with rehydration with H_2O.

dx.doi.org/10.1021/ic501581c | Inorg. Chem. 2014, 53, 9932−9945

The IR spectrum of this compound shows a peak at 2600 cm^{-1} correlating to the D−O stretching and no peak at 3500 cm^{-1} correlating to H_2O, indicating the formation of $\mathbf{3d_8}$. This isotopomer can also be made directly by using D_2O in the original preparation. This cycling of $\mathbf{3} \rightarrow \mathbf{4} \rightarrow \mathbf{3d_8}$ and $\mathbf{3d_8} \rightarrow \mathbf{4d_2} \rightarrow \mathbf{3}$ showed conclusively that there is an exchange between the coordinated water and the interstitial waters of **3** during the breathing, even though the compound that forms upon dehydration, **4**, retains the coordinated water. The ^{1}H NMR spectrum of both of **3** and of **4** are similar, with the only difference the integration of the resonance around 4.5 ppm, which is attributed to the water. This resonance assignment was confirmed by the ^{2}H NMR spectra of $\mathbf{3d_8}$. In contrast, the ^{13}C NMR spectra of the two compounds are very different and clearly identify the compounds. We note an interesting and potentially confusing observation while obtaining the ^{2}H NMR spectra of $\mathbf{3d_8}$. The initial spectrum of the as-prepared sample of $\mathbf{3d_8}$, synthesized from deuterated solvents but not vacuum-dried to prevent the formation of **4**, was unexpected as it showed a sharp component nearly drowning out the broader signal from the compound. The sharp component was determined to arise from adsorbed water on the crystals from the solvothermal synthesis. After vacuum/hydration cycling the crystals, $\mathbf{3d_8} \rightarrow \mathbf{4d_2} \rightarrow \mathbf{3d_8}$, the adsorbed water was absent and the ^{2}H NMR spectra had only one resonance, showing that the sharp resonance was indeed the adsorbed water. These experiments also show that the coordinated water could not be distinguished from the interstitial waters by either IR or ^{2}H NMR.

Like most compounds with a 1,8-naphthalimide moiety, compounds **1**−**5** all exhibit significant solid-state luminescence. The fluorescence maxima for compounds **1** and **3** are red-shifted by 32 and 16 nm, respectively, when compared to the protonated ligand, as expected for a typical ligand-to-metal charge transfer. Interestingly the fluorescence maxima for compounds **2** and **5** are blue-shifted by 34 and 48 nm, respectively. All alkali metal complexes with these same two ligands exhibit the same trend of red-shifted fluorescence maxima for $\mathbf{L_{ala}}^-$ and blue-shifted for $\mathbf{L_{ser}}^-$ complexes. Compound **5**, the only compound containing face-shared polyhedra, exhibits the most blue-shifted maximum of all our compounds to date.[7]

■ ASSOCIATED CONTENT

Ⓢ Supporting Information

Powder X-ray diffraction patterns for compounds **2**−**5**, solution and refinement of single-crystal X-ray diffraction data, and X-ray crystallographic files in CIF format for the structural determinations. This material is available free of charge via the Internet at http://pubs.acs.org.

■ AUTHOR INFORMATION

Corresponding Author

*E-mail: reger@mailbox.sc.edu.

Notes

The authors declare no competing financial interest.

■ ACKNOWLEDGMENTS

The authors acknowledge with thanks the financial support of the Army Research Office (Grant 59042-CH-REP) and the National Science Foundation (Grant CHE-1011736). We thank Dr. Paul Ellis for advice on the solid-state NMR experiments.

■ REFERENCES

(1) (a) Qiu, S.; Zhu, G. *Coord. Chem. Rev.* **2009**, *253*, 2891. (b) Fan, J.; Zhu, H.-F.; Okamura, T.-A.; Sun, W.-Y.; Tang, W.-X.; Ueyama, N. *Inorg. Chem.* **2003**, *42*, 158. (c) de Lill, D. T.; Bozzuto, D. J.; Cahill, C. L. *Dalton Trans.* **2005**, *12*, 2111.

(2) (a) Tranchemontagne, D. J.; Mendoza-Cortés, J. L.; O'Keefe, M.; Yachi, O. M. *Chem. Soc. Rev.* **2009**, *38*, 1257. (b) Rosi, N. L.; Kim, J.; Eddaoudi, M.; Chem, B.; O'Keeffe, M.; Yaghi, O. M. *J. Am. Chem. Soc.* **2005**, *127*, 1504. (c) O'Keeffe, M.; Yaghi, O. M. *Chem. Rev.* **2012**, *112*, 675.

(3) (a) Weber, E., Ed. *Design of Organic Solids*; Topics in Current Chemistry; Springer: Berlin, 1998; Vol. *198*. (b) Pidcock, E.; Motherwell, W. D. S. *Cryst. Growth Des.* **2005**, *5*, 2232. (c) Du, M.; Zhang, Z. H.; Zhao, X. J. *Cryst. Growth Des.* **2005**, *5*, 1199. (d) Takahashi, S.; Katagiri, T.; Uneyama, K. *Chem. Commun.* **2005**, 3658. (e) Weatherhead-Kloster, R. A.; Selby, H. D.; Miller, W. B.; Mash, E. A. *J. Org. Chem.* **2005**, *70*, 8693. (f) Zhang, J. P.; Lin, Y.-Y.; Huang, X. C.; Chen, X.-M. *Chem. Commun.* **2005**, 1258. (g) Vangala, V. R.; Bhogala, B. R.; Dey, A.; Desiraju, G. R.; Broder, C. K.; Smith, P. S.; Mondal, R.; Howard, J. A. K.; Wilson, C. C. *J. Am. Chem. Soc.* **2003**, *125*, 14495.

(4) (a) Murdock, C. R.; McNutt, N. W.; Keffer, D. J.; Jenkins, D. M. *J. Am. Chem. Soc.* **2014**, *136*, 671. (b) Li, G.; Zhu, C.; Xi, X.; Cui, Y. *Chem. Commun.* **2009**, *16*, 2118. (c) Wu, H. N.; Reali, R. S.; Smith, D. A.; Trachtenberg, M. C.; Li, J. *Chem.—Eur. J.* **2010**, *16*, 13951.

(5) (a) Sutrisno, A.; Huang, Y. *Solid State Nucl. Magn. Reson.* **2013**, *49*, 2013. (b) Hoffman, H. C.; Debowski, M.; Müller, P.; Paasch, S.; Senkovska, I.; Kaskel, S.; Brunner, E. *Materials* **2012**, *5*, 2537.

(6) (a) Reger, D. L.; Horger, J. J.; Smith, M. D.; Long, G. J.; Grandjean, F. *Inorg. Chem.* **2011**, *50*, 686. (b) Reger, D. L.; Horger, J. J.; Smith, M. D. *Chem. Commun.* **2011**, *47*, 2805. (c) Reger, D. L.; Horger, J. J.; Debreczeni, A.; Smith, M. D. *Inorg. Chem.* **2011**, *50*, 10225.

(7) (a) Reger, D. L.; Leitner, A. P.; Smith, M. D. *Inorg. Chem.* **2012**, *51*, 10071. (b) Reger, D. L.; Leitner, A.; Smith, M. D.; Tran, T. T.; Halasyamani, P. S. *Inorg. Chem.* **2014**, *52*, 10041.

(8) (a) Rombach, M.; Gelinsky, M.; Vahrenkamp, H. *Inorg. Chim. Acta* **2002**, *334*, 25. (b) Fox, S.; Buesching, I.; Barklage, W.; Strasdeit, H. *Inorg. Chem.* **2007**, *46*, 818.

(9) (a) Reger, D. L.; Debreczeni, A.; Smith, M. D. *Inorg. Chem.* **2011**, *50*, 11754−11764. (b) Reger, D. L.; Debreczeni, A.; Smith, M. D.; Jezierska, J.; Ozarowski, A. *Inorg. Chem.* **2012**, *51*, 1068−1083. (c) Reger, D. L.; Debreczeni, A.; Reinecke, B.; Rassolov, V.; Smith, M. D.; Semeniuc, R. F. *Inorg. Chem.* **2009**, *48*, 8911−8924.

(10) Reger, D. L.; Debreczeni, A.; Horger, J. J.; Smith, M. D. *Cryst. Growth Des.* **2011**, *11*, 4068−4079.

(11) Banerjee, S.; Veale, E. B.; Phelan, C. M.; Murphy, S. A.; Tocci, G. M.; Gillespie, L. J.; Frimannsson, D. O.; Kelly, J. M.; Gunnlaugsson, T. *Chem. Soc. Rev.* **2013**, *42*, 1601.

(12) (a) Fromm, K. M. *Coord. Chem. Rev.* **2008**, *252*, 856. (b) Banerjee, D.; Parise, J. B. *Cryst. Growth. Des.* **2011**, *11*, 4704.

(13) Appelhans, L. N.; Kosa, M.; Radha, A. V.; Simoncic, P.; Navrotsky, A.; Parrinello, M.; Cheetham, A. K. *J. Am. Chem. Soc.* **2009**, *131*, 15375.

(14) Duer, M. J. *Introduction to Solid-State NMR Spectroscopy*; Blackwell Publishing, Inc., Oxford, U.K., 2004.

(15) (a) Mallick, A.; Saha, S.; Pachfule, P.; Roy, S.; Banerjee, R. *J. Mater. Chem.* **2010**, *20*, 9073. (b) Appelhans, L. N.; Kosa, M.; Radha, A. V.; Simoncic, P.; Navrotsky, A.; Parrinello, M.; Cheetham, A. K. *J. Am. Chem. Soc.* **2009**, *131*, 15375. (c) Yeung, H. H.-M.; Kosa, M.; Parrinello, M.; Forster, P. M.; Cheetham, A. K. *Cryst. Growth Des.* **2011**, *11*, 221. (d) Rood, J. A.; Noll, B. C.; Henderson, K. W. *J. Solid State Chem.* **2010**, *183*, 270. (e) Gao, Q.; Wang, X.; Conato, M. T.; Makerenko, T.; Jacobson, A. *J. Cryst. Growth Des.* **2011**, *11*, 4632.

(16) Bertke, J. A.; Oliver, A. G.; Henderson, K. W. *Inorg. Chem.* **2012**, *51*, 1020.

(17) Reger, D. L.; Debreczeni, A.; Reinecke, B.; Rassolov, V.; Smith, M. D.; Semeniuc, R. F. *Inorg. Chem.* **2009**, *48*, 8911.
(18) (a) Thomas-Gipson, J.; Beobide, G.; Castillo, O.; Cepeda, J.; Luque, A.; Pérez-Yáñez, S.; Aguayo, A. T.; Román, P. *Cryst. Eng. Comm* **2011**, *13*, 3301. (b) Nugent, P. S.; Rhodus, V. L.; Pham, T.; Forrest, K.; Wojitas, L.; Space, B.; Zaworotko, M. J. *J. Am. Chem. Soc.* **2013**, *135*, 10950.